University of Baghdad
College of Engineering
JOURNAL OF ENGINEERING

Journal of Engineering

journal homepage: www.jcoeng.edu.iq

Volume 32 Number 7 July 2026

Fabrication and Mechanical Characterization of HDPE Composites Reinforced with Waste Polyester Fibers and Recycled HDPE

Huda A Abdulimam *, Hayder A Abbood

Department of Materials Engineering, College of Engineering, University of Basrah, Basra City, Iraq

ABSTRACT

Waste polyester fibers (WPFs) were used to prepare a range of high-density polyethylene (HDPE) composites with maleic anhydride-grafted polyethylene (PE-g-MA) as compatibilizer, and these were characterized. The objective of the research was to enhance the mechanical properties of HDPE and to encourage the use of plastic and textile waste. The composite specimens were made using single-screw extrusion, and tensile, flexural, impact, differential scanning calorimetry (DSC), density, porosity, and water absorption were measured. A systematic evaluation of fiber orientation and recycled HDPE (r-HDPE) content was made. The results showed that the fiber orientation had a significant influence on the stress transfer and failure mechanisms. The mesh-reinforced composite configuration had the best overall performance with tensile strength of 52 MPa and impact strength of 487.8 J/m, while the aligned fiber configuration had the highest flexural strength of 104.7 MPa. PE-g-MA was added, which increased the adhesion between the fiber and the matrix and decreased the void formation. With the gradual incorporation of r-HDPE, the mechanical properties were gradually reduced because of the degradation of the polymer and reduction in interfacial interactions, but the composites with up to 15 wt.% r-HDPE still performed well. The results show that the use of polyester fiber-reinforced HDPE waste composite represents a viable approach to producing high-quality engineering materials with high recycled content and improved mechanical properties.

Keywords: HDPE, Recycled HDPE, Recycled plastics, Waste polyester fibers.

1. INTRODUCTION

Fiber-reinforced polymers (FRPs) consist of a matrix and high-strength fibers, where the matrix serves as a lightweight medium that enhances the overall mechanical performance of the composite **(Ajayi et al., 2025)**. The incorporation of natural or synthetic fibers, such as polyester, into high-density polyethylene (HDPE) significantly improves tensile strength, rigidity, and environmental sustainability. These composites are extensively utilized in the automotive, aerospace, construction, and packaging sectors due to their favorable strength-

*Corresponding author
Peer review under the responsibility of University of Baghdad.
https://doi.org/10.31026/j.eng.2026.07.10

Article received: 14/05/2026
Article revised: 03/06/2026
Article accepted: 03/06/2026
Article published: 01/07/2026

to-weight ratios and eco-friendly characteristics **(Al-Obaidi, 2023)**. Furthermore, reinforced HDPE has found applications in demanding marine environments, including intelligent sea pontoons, which necessitate exceptional durability and corrosion resistance under aggressive physical conditions **(Awad et al., 2019)**. **(Edah et al., 2025)** emphasizes the utilization of plastic waste to enhance composite properties while simultaneously mitigating environmental pollution. Given that polyester accounts for approximately 57% of global fiber production, its recycling is paramount for the sustainability of the textile industry **(Housmans et al., 2009)**. However, achieving robust interfacial bonding remains a significant challenge due to the inherent polarity differences between hydrophilic fibers and hydrophobic matrices **(Kantz et al., 1972)**. The accumulation of HDPE waste poses severe environmental risks, necessitating sustainable recycling strategies **(Ragaert et al., 2017)**. Recycled HDPE (r-HDPE) typically exhibits diminished performance compared to virgin material due to thermal and shear degradation during reprocessing **(Zeng et al., 2025).**

Extrusion molding involves shear and compression stresses acting on the polymer melts, which promote the formation of semi-crystalline structures and influence the mechanical properties of the final composite **(Chen et al., 2020)**. Reprocessed plastics, however, undergo substantial chain scission and degradation due to the cumulative effects of thermal and mechanical stresses **(Douiri et al., 2024; Kaneyasu et al., 2021)**. These effects are often exacerbated by impurities and structural defects, leading to compromised mechanical properties. Although fiber reinforcement is an established strategy to mitigate these weaknesses **(Joseph et al., 1996; Asyraf et al., 2022)**, a significant research gap remains regarding the use of structured mesh architectures combined with PE-g-MA compatibilizers to optimize composite performance **(Chen et al., 2024)**.

Although PE-g-MA compatibilization and polyester fiber reinforcement have been extensively investigated, limited attention has been given to structured mesh architectures as a reinforcement strategy for recycled HDPE composites. To address this research gap, a mesh-based reinforcement architecture was developed and evaluated in the present study. The novelty of the mesh fiber architecture investigated in this work lies in its interconnected reinforcement network, which fundamentally differs from conventional random or discontinuous fiber arrangements. Unlike traditional methods, the mesh structure provides multiple load-transfer pathways and promotes a more uniform stress distribution throughout the composite. Recent advancements in composite science have emphasized that the architecture of the reinforcement network is a critical determinant of fracture response and crack-growth resistance **(Fox et al., 2025; Venkat Ramanan and Rajamurugan, 2024).** By implementing an interconnected mesh, this study aims to hinder crack propagation and enhance energy absorption by increasing crack-path complexity within the woven framework, a mechanism recently highlighted for its effectiveness in reinforced composite laminates **(Benhamadouche et al., 2025).** This structured approach offers a robust and effective strategy for utilizing waste polyester fibers as a continuous reinforcing framework in recycled HDPE systems, addressing the limitations of traditional discontinuous reinforcement.

Consequently, this study was conducted to optimize the compositions of waste HDPE/polyester fiber using mix-design techniques, focusing on the characterization of mechanical, thermal (DSC), and morphological (SEM) properties to formulate cost-effective, high-performance composites for sustainable material development.

2. MATERIALS AND METHODS

2.1 Materials

The State Company provided v-HDPE of SCPILEX EHM 6003 grade for Petrochemical Industries (SCPI), Basra, Iraq. And recycled material derived from wastewater bottle caps made of HDPE, from JUSTER, long strands of PF, and from the polyester tow straps. Either as continuous filaments added separately to the melt or broken fibers pre-blended with polyethylene pellets. Polyethylene grafted with maleic anhydride, acting as a crosslinking agent (Jianxing, China), with a grafting concentration. This compatibilizer was chosen because of its ability to form physical or chemical interactions with functional groups on the fiber surface, which leads to interfacial tension between phases being reduced. The physical and mechanical properties of baes materials and reinforcements are provided in **Table 1**. This study examined the available colors of raw materials, as shown in **Fig. 1**.

Table 1. Mechanical and Physical Properties of Composite Constituents

Property	**HDPE**	**PF**	**PE-g-MA**
Melting Point (^oC)	128-137	250-260	80-125
Density, ρ (g/cm^3)	0.963	1.38	0.916
Tensile Strength, σ (MPa)	30	167	16.50
Tensile Modulus, E (GPa)	1.585	10.00	0.600
Elongation, ε_f (%)	> 600	7	7
Poisson's Ratio, ν	0.45	0.35	0.42

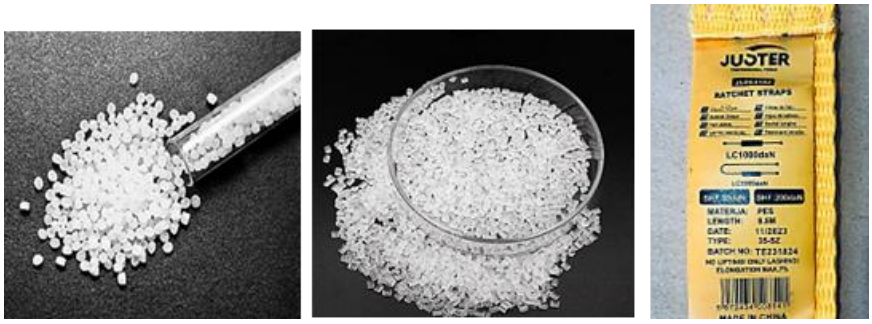

(a) (b) (c)

Figure 1. Raw materials used (a) HDPE, (b) PE-g-MA, and (c) PF

In fact, we chose PE-g-MA 4 wt% compatibilizer due to a specific literature review, and it has been reported to improve performance in the case of similar composite systems. The research on the recycling of the high-density polyethylene and poplar fiber composites showed that the addition of PE-g-MA concentration of 2 and 4 wt% increased the stability and mechanical properties. Even the tensile strength was further enhanced than that of the composites, which lacked the compatibilizing agent **(Kazayawoko et al., 2009).** This finding is in support of using 4 wt % in our formulation as a sure way to as an effective approach to enhance the fiber-matrix interfacial adhesion, and higher mechanical performance is achieved. According to the general literature, compatibilizer concentrations between 2 and 12.5 wt% have been shown to work well in HDPE-fiber composites **(Grande and Torres, 2005; Lima et al., 2017; Prajapati et al., 2017)**. The concentration was chosen based on the initial optimization experiment and the overall processing conditions of similar polymer composites **(Savas et al., 2016).** The screw speed of 60 rpm was calculated for the single-

screw extrusion process. In fact, other studies have used screw speeds of 10-50 rpm in making HDPE-wood composites; however, this study employed a higher speed of 60 rpm to ensure that the polyester fibers were well mixed with the HDPE material. Essentially, they kept the speed at a low level as they did not want the polymer and fibers to be damaged by heat whilst sustaining the same good processing rate and quality of fibers **(Wilczyński et al., 2018; Xiao and Tzoganakis, 2010).**

One-way analysis of variance (ANOVA) was used to statistically analyze the results of the means of various composite formulations to determine significant differences between the means. All the statistical tests were performed at a level of significance of $p < 0.05$. All mechanical properties were calculated to give mean values and standard deviations.

2.2 Preparation of Composites

The composites were made by extrusion with a base formulation of 86 wt.% HDPE and 10 wt.% polyester fibers (PF) with 4 wt.% PE-g-MA compatibilizer. Virgin HDPE was partly replaced by r-HDPE for the recycled composites with amounts of 5 to 30 wt.%. Various reinforcement configurations were explored, such as 0°, 30°, 45°, 60°, 90°, short fibres, random fibres, and mesh structures. The high strength and durability of waste polyester fibers (WPF) recovered from industrial lifting belts (1000 daN, elongation <7%) were used as reinforcement in the composite matrix. The composite was fabricated from a single screw extruder (L/D ratio = 25:1) at a fixed screw speed of 60 rpm and a batch weight of 1000 g. The temperatures for each of the four heating zones were kept at 180, 190, 220, and 240 °C. The polyester fibers were preheated for 3 min before processing in order to enhance the interfacial adhesion. The extruder featured a screw diameter of 25 mm, with a residence time of approximately 3 min. After processing, the molten composite was cast into a custom perforated aluminium mold and allowed to solidify at ambient temperature (23 ± 2 °C).

Although dynamic rheological characterization was not conducted in the present study, the melt flow index (MFI = 0.3 g/10 min) of the HDPE matrix was sufficient to ensure a stable process and keep the integrity of the mesh reinforcement during the extrusion and casting process.

The fiber orientations (0°, 30°, 45°, 60°, 90°, and mesh) were obtained by using a custom perforated aluminum mold. In order to ensure the accurate positioning and mechanical fixing of fibers, pre-drilled holes with a spacing of 1 cm were prepared in the mold. The fibers were manually threaded through the designated holes corresponding to each orientation before mechanical fixation. In the case of the mesh architecture, the reinforcement was designed to create a compact, interconnected mesh with openings of about 2–3 mm and polyester yarns with an average thickness of 1 mm. To ensure that the reinforcement network did not move during the processing, it was mechanically fixed inside the mold before the injection of the melt. The molten composite was then poured into the mold and cooled according to a pre-programmed cooling schedule.

2.3 Characterization

The composites prepared had been evaluated for their mechanical properties. Tensile strength and Young's modulus were determined according to **(ASTM D638, 2014)**. The experimental specimens, depicted in **Fig. 2**, were the Type I. A universal testing machine (Model: LR-WDW-10KN, Dongguan Lonroy Equipment Co., Ltd.) was used to conduct all the experiments under a constant tensile rate of 5mm/min. The results presented were an average of at least five specimens for each mixture**(ASTM D638, 2014).** Flexural properties

were investigated from a three-point bending test according to **(ASTM D790, 2010)**. **Fig. 3** shows the standard dimensions of the flexural specimens. Flexural strength and modulus tests were carried out using the same universal testing tool (Model LR-WDW-10KN) at a rate of 2 mm/min. Results can be had with no less than 5 replicates per mixture. Impact resistance of the specimens was evaluated in accordance with **(ASTM D256, 2010)**(Izod method). The experiment was performed on the notched samples to obtain the energy needed to fracture with the geometry as shown in **Fig. 4**. They were measured using an impact testing instrument (Model BROOKS MAT 21/D50 Brooks Inspection Equipment Ltd. Note that these results were an average of at least five specimens per mixture**.**

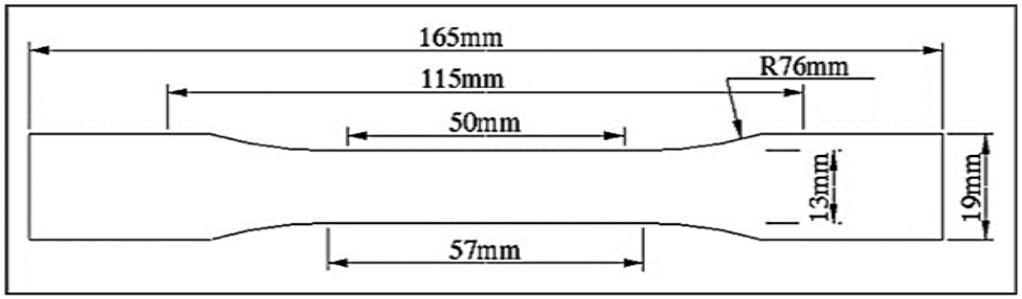

Figure 2. The tensile sample according to **(ASTM D638, 2014)**

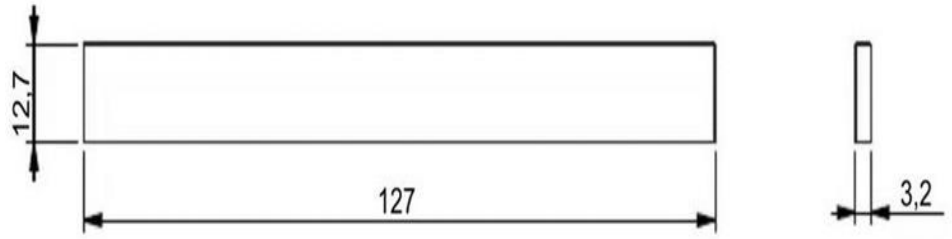

Figure 3. The flexural sample according to **(ASTM D790, 2010)**

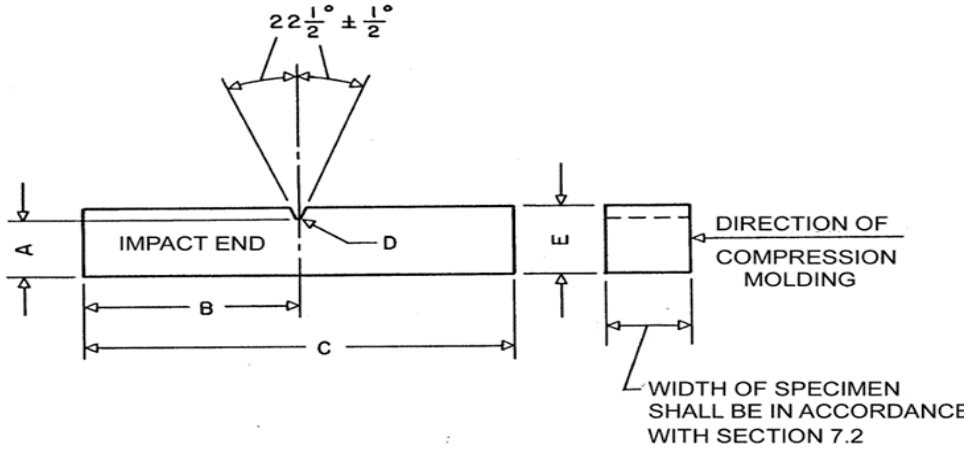

Figure 4. The impact sample according to **(ASTM D790, 2010)**

The Inspect™ F50 SEM (FEI Company, USA) was used for surface morphology and interfacial adhesion studies, and the samples were gold-coated to provide conduction. The thermal properties were examined by heating the sample from room temperature to 200 °C at a rate of 5 °C/min using DSC-60 (Shimadzu, Japan). The procedure was performed under a nitrogen atmosphere (50 mL/min) to avoid oxidation and get accurate thermal data.

2.4 Apparent Density and Porosity Test

The apparent density of the HDPE reinforced samples was determined using **(ASTM D1895-96, 2010)** standard, as confirmed in the study of **(Choi et al., 2006).** Equation 1 was applied to find the boards' apparent densities. The average of the five boards' test results was used to represent the apparent density.

$$\text{Apparent density (gm/cm}^3) = \frac{m_o}{V} \quad (1)$$

where V is the board's volume (cm^3), and m_o is the mass (g) measured using a high-accuracy digital balance scale.

Apparent porosity (Pa), defined as the ratio of open pore volume to the total exterior volume, was determined using Archimedes' principle according to the GB/T1966-1996 standard **(Ma et al., 2008)** and the methodology of **(Liu et al., 2019).** The experimental procedure involved drying the samples at 90 °C until a constant dry mass (Md) was achieved. Subsequently, the samples were boiled in distilled water for 120 minutes to ensure saturation. The saturation weight in air (Ms) and the immersion weight in water (Mi) were then recorded, and the apparent porosity was calculated using Eq. (2):

$$P_a(\%) = \frac{M_s - M_d}{M_s - M_i} \times 100 \quad (2)$$

2.4.1 Moisture Absorption Property

Moisture absorption was tested according to **(ASTM D570, 2018)**. For each treatment, five samples measuring 10 × 10 × 3 mm were evaluated. The specimens were first dried to remove the moisture before the test, and to get the initial weight constant, the moisture was removed by drying at 50 °C for 24 h. The samples were then placed in distilled water at 23 ± 2 °C and weighed after 24 h and then at regular intervals for 7 days to track the moisture uptake and saturation behavior. All surface water was carefully removed with a lint-free absorbent cloth before each weighing, thus only absorbed water was weighed.

The water absorption percentage was determined by calculating the weight difference between the dry and saturated samples using the following Equation:

$$\Delta M(\%) = \frac{M_f - M_i}{M_i} \times 100 \quad (3)$$

where ΔM (%) is the moisture uptake, M_f and Mi are the mass of the specimen after and before immersion.

2.4.2 Density

Fig. 5. Density of v-HDPE and some waste polyester fiber-reinforced combinations. Since density and porosity influence mechanical properties to a large extent **(Gupta and Singh, 2019)**, these important parameters were carefully monitored. The density of the v-HDPE was 0.963 g/cm^3, while samples with 5–30% r-HDPE and PF in either direction showed 10% and 3 %, respectively, reductions in density. These reductions are mainly due to voids or air trapping occurring during the processing **(Asim et al., 2018; Jawaid et al., 2011)**.

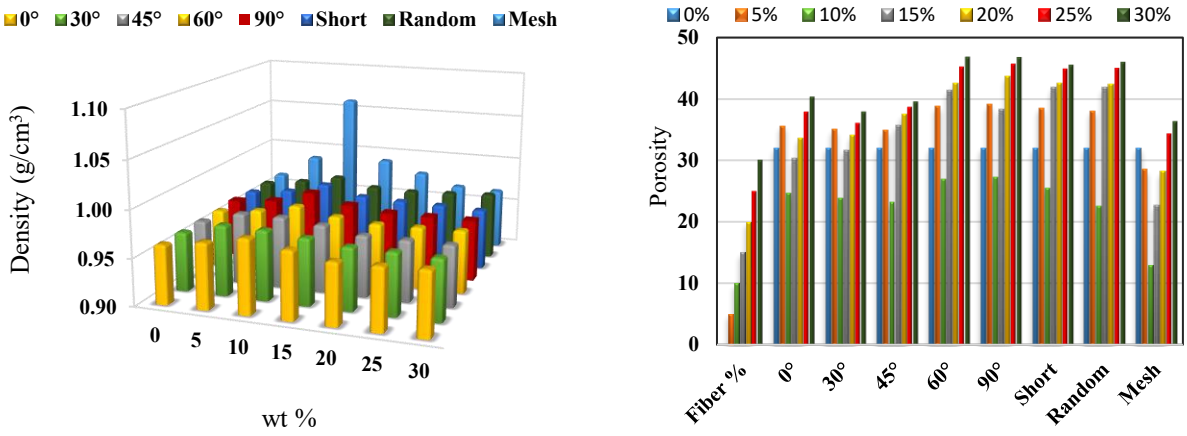

(a) (b)

Figure 5. The density and porosity of reinforced composites: (a) Density and (b) Porosity.

Fiber concentration, fiber length, and processing significantly contribute to the apparent porosity of HDPE composites due to thermo-mechanical degradation. As indicated in **Fig. 5b**. The configuration with 10 % fiber mesh noticeably reduced porosity. This improvement suggests that the presence of PE-g-MA and the polyester fiber mesh may improve interfacial compatibility, which improves fiber distribution among each other while making them more compatible at their interfacial areas, as has been confirmed by Yamsaengsung and Sombatsompop **(Yamsaengsung and Sombatsompop, 2009).** In addition, the porosity trends demonstrate an obvious relationship between 10 % mesh-reinforced samples with different amounts of r-HDPE waste or recycling rates.

2.4.3 Water Absorption

Water absorption (WA) in reinforced HDPE was measured as a function of porosity and is shown in **Fig. 6.** HDPE alone exhibited low WA (<0.05%), but this increased to 0.52 % when fibers were incorporated. In particular, very low uptake (0.03%) was observed for mesh composites having grafted anhydride polyethylene. It is affected by interfacial adhesion and also determines the properties of fibers, orientation, and voids **(Jawaid et al., 2019).** The hydrogen-bonding interaction between water and carboxylic/ester groups encourages interfacial diffusion, which agrees with **(Ngaowthong et al., 2019)** and standard fibre-reinforced HDPE composites **(Singh Bahra et al., 2017).**

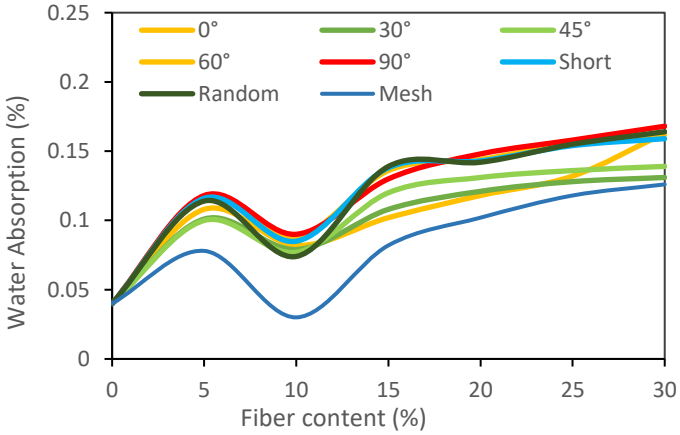

Figure 6. The Water Absorption with Fiber Content (All Orientations)

3. RESULTS AND DISCUSSION

3.1 Mechanical Properties Analysis

Evaluated PF content (5, 10, 15, and 20%) for HDPE mechanical performance is listed in **Table 2.** The load transfer was optimal, yet tensile stress peaked to 23.4 MPa along 10 % PF. Limited distributions of each fiber type at earlier time points led to concentrations between 15–20 %, which resulted in saturation (23.1 MPa) or near-saturation and decreases. As a result, 10 % PF was chosen as the optimal ratio for improved mechanical strengthening, structural uniformity, and manufacturability.

Table 2. Fiber ratio values

Polyester (%)	**5**	**10**	**15**	**20**
Tensile Stress (MPa)	22.0	23.4	23.4	23.1

Fig. 7 demonstrates that the mesh-reinforced configuration achieved the highest tensile strength of 52 MPa, a 126 % increase over unreinforced HDPE (23 MPa). This performance is driven by the structure's high density (1.061 g/cm^3) and minimal porosity (13%), which reduces internal stress concentrators. An efficient transfer of stress, achieved by strengthening the interfacial shear strength via interfacial interaction, may be associated with the presence of PE-g-MA compatibilizer. The unidirectional fibers are also anisotropic in nature, as their strength is reduced when the orientation angle from 0° to 90°. Mesh design offers biaxial reinforcement. Such synergy between structural design and chemical compatibilization helps achieve better stress dispersion, thereby reducing the adverse effects of off-axis debonding and anisotropy. The enhanced mechanical performance of the mesh-reinforced composites is associated with the combined action of improved interfacial adhesion related to the presence of PE-g-MA and the efficient stress-transfer network created by the mesh architecture. Statistical analysis using One-way ANOVA confirmed that fiber architecture significantly influenced the mechanical properties ($p < 0.0001$). This behavior is supported by the established role of PE-g-MA in stabilizing interfacial compatibility **(Prajapati et al., 2017)** and the recognized significance of mesh reinforcement in optimizing stress distribution and structural integrity **(Venkat Ramanan and Rajamurugan, 2024).**

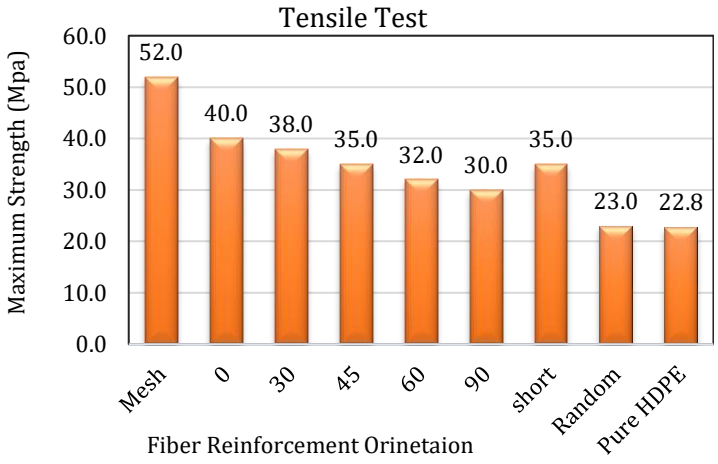

Figure 7. Ultimate tensile strength of the composites with different fibre reinforcement types

The tensile strength results showed that there are considerable differences in the tensile strength of the composite configurations examined. The mean values with standard deviation of tensile strength are summarized in **Table 3**. One-way ANOVA revealed that tensile performance is significantly different with respect to reinforcement architecture ($F(8,36) = 142.56$, $p < 0.001$). The tensile strength of the mesh-reinforced configuration was found to be the highest (52.0 ± 1.8 MPa), and was significantly higher than the other fibre architectures investigated, based on the Tukey's post-hoc analysis. This attribute is attributed to the biaxial reinforcement mesh which has a structure that prevents the generation of excessive stress concentration when loading and spreads it out. Hence, it can be concluded that the best tensile reinforcement of the composites studied was the mesh design.

Table 3. ANOVA analysis of tensile strength

Standard Deviation	Mean	Category
1.8	52	Mesh
1.2	40	0
1.1	38	30
1.0	35	45
0.9	32	60
0.8	30	90
1.0	35	Short
0.7	23	Random
0.6	22.8	Pure

As shown in **Fig. 8**, the maximum flexural strength of 104.70 MPa was achieved for the 0° up to a value significantly higher than that of the unreinforced specimen (40.11 MPa), by an increase factor of about +161%. The favorable effect of the low water absorption (0.03 % for 10 % mesh, **Fig. 6**) on the stability of the mesh and 0° setups can be attributed to the increasing dominance of PE-g-MA's potential to improve fiber–matrix interaction . It delays damage from moisture diffusion in the fiber matrix bond and premature pull-out of the fibers. Increased interfacial bonding assists in withstanding the transverse bending stresses, providing us with uniform load transfer from matrix to fiber network

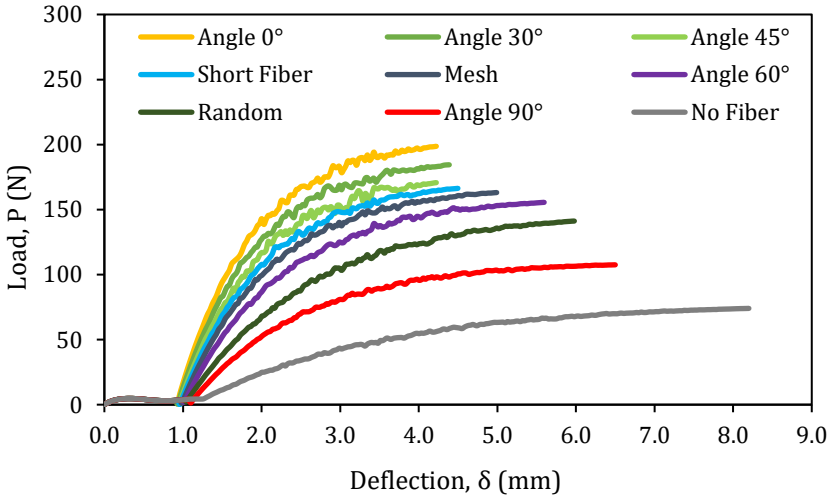

Figure 8. Flexural strength with different fiber reinforcement.

The flexural strength results showed marked differences between the different fiber architectures studied. **Table 4** shows the results of one-way ANOVA testing for the effect of reinforcement configuration on flexural performance, which was found to be statistically significant ($F(8,36) = 353.43$, $p < 0.001$). There were significant differences between the investigated fiber architectures based on Tukey's post-hoc analysis, with the 0° orientation having the highest flexural strength (104.7 ± 3.1 MPa). This is related to the parallel arrangement of fibers with the loading direction, which results in better load transfer and resistance to bending stresses. Off-axis orientations, on the other hand, showed lower bending flexural strength because the reinforcement was less effective in bending. Hence, the composite configuration 0° had the most desirable flexural response of the composites analyzed.

Table 4. ANOVA results for flexural strength

Standard Deviation	Mean	Category
2.5	85.78	Mesh
3.1	104.7	0
2.8	96.35	30
2.6	89.12	45
2.4	82.41	60
1.6	55.8	90
2.6	88.4	Short
2.2	75.66	Random
1.2	40.11	Pure

The Izod impact strength of the composite with mesh reinforcement was determined to be 487.8 J/m (138% above unreinforced v-HDPE, **Fig. 9**). This enhancement is due to the simultaneous directional anti-propagation of cracks in each direction by the mesh, combined with low porosity, which prevents high-speed propagation of cracks. With kinetic energy mainly dissipated due to fiber bridging and moderate interfacial debonding at the same time, this is attributed to the unique synergy between mesh architecture and PE-g-MA bonding. The system reduces the risk of catastrophic fracture and dramatically enhances impact resistance by guiding cracks into convoluted paths that increase the energy needed for failure.

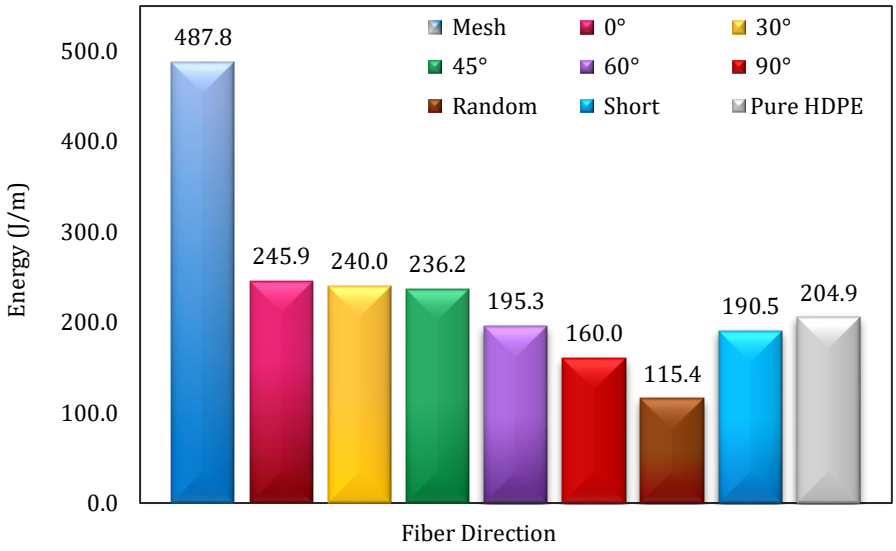

Figure 9. Izod impact strength for the composite with different fiber reinforcement types

Statistical analysis was conducted for impact properties to assess whether the observed differences in the different fiber architectures investigated are significant. The mean impact strength values and standard deviations are shown in **Table 5**. The one-way ANOVA gave statistically significant results, which indicated that reinforcement architecture had a significant effect on impact performance ($F(8,36) = 980.39$, $p < 0.001$). The results of Tukey's post hoc analysis revealed that there were statistically significant differences between the different configurations investigated, with the mesh-reinforced composite having the highest impact strength (487.8 ± 14.6 J/m). This behavior is associated with the interconnected reinforcement network of the mesh structure, leading to energy dissipation and resistance to crack propagation under impact loading. The unidirectional, short-fiber and random fiber configurations. Therefore, the mesh architecture exhibited the most favorable impact response among the investigated composite designs.

Table 5. ANOVA analysis of Impact strength

Standard Deviation	Mean	Category
14.6	487.8	Mesh
7.4	245.9	0
7.2	240	30
7.1	236.2	45
5.8	195.3	60
4.8	160	90
5.7	190.5	Short
3.4	115.4	Random
6.1	204.9	Pure

In the second part of this study, the effect of r-HDPE content was evaluated as summarized in **Table 6.** Across the whole r-HDPE levels up to 30%, a distinct decline in mechanical performance was recorded. Specifically, the tensile strength decreased from 52 MPa to 20 MPa, and the flexural strength dropped from 85.78 MPa to 71.11 MPa. In a similar manner, the impact decreased from 487.8 J/m to 314.9 J/m as observed, indicating that recycled content seriously affects the overall properties of composite materials.

Table 6. Mechanical properties of the mesh-reinforced composites with different recycled HDPE content

Waste %	Tensile Strength (MPa)	Flexural Strength (MPa)	Izod (J/m)
0%	52	85.78	487.80
5%	38	85.50	454.51
10%	31	84.10	390.60
15%	29	82.11	381.70
20%	25	78.45	320.00
25%	22	74.78	317.46
30%	20	71.11	314.90

Mechanical degradation is intrinsically related to the apparent change of morphology shown in **Fig. 5.** Density rises to 0.972 g/cm^3, goes down from the packing effect at 5 % waste, but falls back further to 0.965 g/cm^3 at a loading of 30%, while porosity increases to 26.4 % and water absorption reaches its peak at 0.188 %. The short polymer chains and impurities produce a porous heterogeneous matrix that contributes to stress concentration, leading to premature cracking. The eventual high

impurity levels and molecular degradation in the r-HDPE surpass bonding at the interfacial level, resulting in early rupture of the composite even with the use of a PE-g-MA compatibilizer, leading to a decrease in energy dissipation. Therefore, as recyclability increases, the micro- and macrostructure damage and mechanical performance of the composite material seriously deteriorate.

Table 7. ANOVA results for the mechanical properties of HDPE

Tensile		Flexural		Impact		Waste Percentage
Standard Deviation	Mean	Standard Deviation	Mean	Standard Deviation	Mean	
1.5	38	2.5	85.5	18.0	454.51	5
1.2	31	2.4	84.1	15.0	390.6	10
1.1	29	2.3	82.11	14.5	381.7	15
1.0	25	2.2	78.45	12.0	320	20
0.9	22	2.1	74.78	11.5	317.46	25
0.8	20	2.0	71.11	11.0	314.9	30

The mechanical performance of composites containing different recycled HDPE was statistically evaluated, as presented in **Table 7**, and the results indicated that recycled HDPE content had a statistically significant effect on the mechanical properties ($p < 0.001$). A substantial decrease was noted for tensile strength ($F(5,24) = 177.55$), from 38 MPa for 5 wt.% r-HDPE to 20 MPa for 30 wt.% r-HDPE. The reduction is correlated with the degradation that is common to recycled polymers as presented in the DSC and SEM analysis. There was also considerable variation in flexural strength ($F(5,24) = 30.95$), but this was not as rapid, ranging from 85.5 MPa to 71.11 MPa. In comparison, the impact strength was most sensitive to recycled material ($F(5,24) = 81.57$), as it was reduced from 454.51 J/m to 314.9 J/m with the increase in r-HDPE content. Increased matrix heterogeneity and micro-void formation were observed under SEM at higher recycling levels, which could have an impact-on-impact performance reduction. Overall, the results show that the composites' mechanical properties can be affected by increasing the recycled HDPE content, and that the mesh-reinforced structure remained effective throughout the investigated composition.

3.2 Microstructural Analysis

Internal structure and fracture planes of composites were examined with an Inspect F50 SEM. **Fig. 10** displays the reference composite (0% waste). At low magnification (**Fig. 10a**), it has an extremely uniform appearance. All this is in agreement with its physical features: the highest density (1.061 g/cm^3) and the lowest porosity (13%). Macroscopic observation (**Fig. 10b**) at a higher magnification reveals that there are no detectable interfacial gaps or fiber pull-outs within the polyester fibers in the HDPE matrix. This interfacial bonding is also consistent with the presence of PE-g-MA, which is known to be used to enhance the compatibility between the HDPE matrix and polyester fibers, leading to stress transfer across the interface. While the enhanced interfacial adhesion in the SEM micrographs and mechanical characteristics of this composite are a convincing indication of the positive effect of PE-g-MA, the mechanism of compatibilization was not directly examined in the present study. Hence, its effect was deduced from the mechanical, morphological and thermal observations. This is also consistent with the low porosity values, which are important to have efficient load transfer and consequently the improved mechanical performance of the reference composite, as the SEM micrographs do not show large pores.

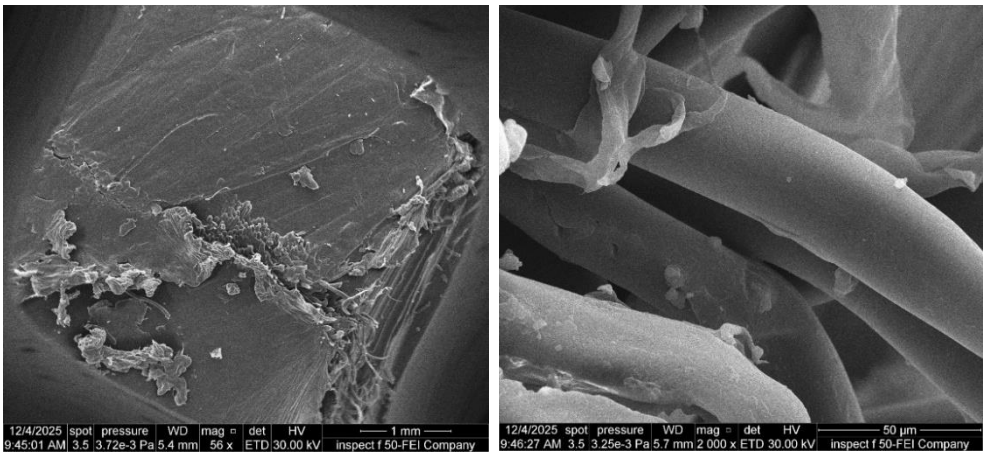

(a) (b)

Figure 10. F50 SEM inspection of the reference composite (0% waste): (a) 56× magnification and (b) 2000× magnification.

However, there is a significant difference in the morphology of the composite with 30% r-HDPE in comparison to that of other composites, as shown in **Fig. 11.** Although the fibres did not appear to be separated from the matrix, microstructures were still significantly less homogeneous, having both polymer agglomerates and many micro-voids. These microstructural variations are in line with the higher porosity (up to 26.4%) and the lower density (0.965 g/cm^3) observed. The micro-voids serve as stress concentrators, which enable the crack to start and propagate through the matrix. In addition, the higher water absorption of 0.188% also indicates less interfacial integrity between the fibers and the matrix, thus reducing the mechanical performance. In general, the mechanical behavior of the recycled composites is well supported by the SEM observations. The compact morphology of the reference composite promotes more efficient stress transfer, while the presence of porosity and heterogeneity in the structure of the recycled composites creates a concentration of stresses and the appearance of cracks at an early stage. For some specimens, complete brittle fracture surfaces were not achieved due to the ductile nature of the HDPE matrix. Thus, SEM examination was done on the failed and deformed areas of the composites. The morphology of the observed failures suggested that failure was dominated by the transfer of stress at the interfaces, deformation of the matrix and crack initiation at micro-voids and heterogeneous zones. These characteristics increased as the r-HDPE content increased and aligned with the observed decreases in tensile strength, flexural strength and impact resistance.The degradation with higher r-HDPE content is consistent with the polymer degradation phenomena, including chain scission, accumulation of impurities and decrease of molecular entanglement. These mechanisms were assessedindirectly rather than by direct molecular or rheological characterization, however, by using SEM, DSC, and mechanical analyses.

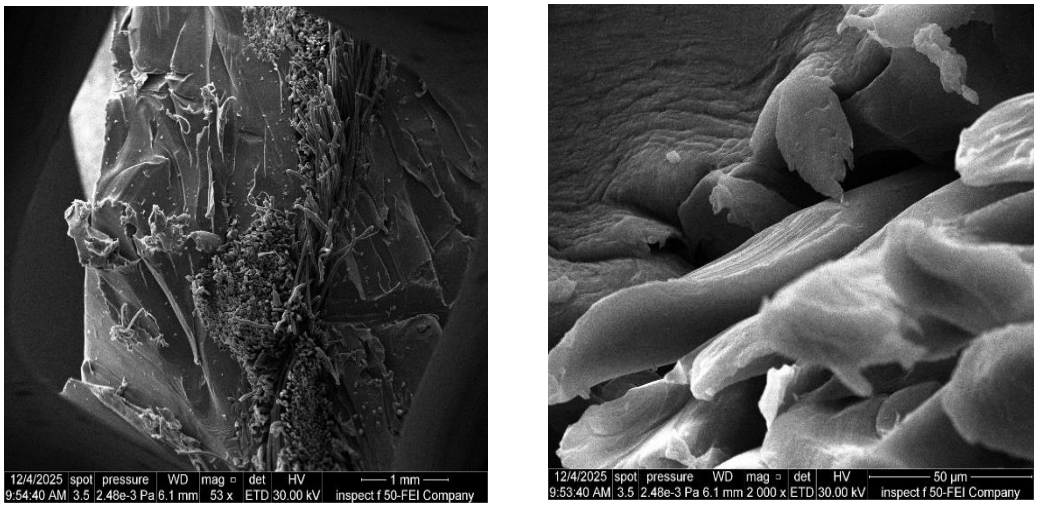

(a) (b)

Figure 11. F50 SEM inspection of the composite containing 30% r-HDPE (30% waste): (a) 53× magnification and (b) 2000× magnification.

3.3 DSC Analysis

The differential scanning calorimetry (DSC) examination of v-HDPE and the final composite (HDPE/PF/PE-g-MA) is presented in **Fig. 12.** The melting point (Tm) was 141.1 °C with a degree of crystallinity (Xc) of 67 % for v-HDPE. In contrast, r-HDPE exhibited reduced Tm (132.3 °C) and a significantly lower Xc of 38.05 % attributed to molecular degradation and chain scission during the recycling process. The final composite maintained a stable Tm of 142.3 °C, while its heat of fusion (110.5 J/g) confirmed the lower crystallinity in the overall composite composition.
The degree of crystallinity (Xc) was calculated from the melting enthalpy obtained from the DSC thermograms using a reference heat of fusion of 293 J/g for fully crystalline HDPE.

$$c = \frac{\Delta H_m}{(1-w).\Delta H_m^o} \cdot 100\% \quad (4)$$

Where ΔH_m is the measured heat of fusion, ΔH^0_m is the heat of fusion of 100% crystalline HDPE, and w is the weight fraction of fibers in the polymer matrix.
In the case of the HDPE/PF/PE-g-MA composite, the crystallinity remained relatively low (≈37.7%), suggesting that the crystallinity of the system was controlled by the recycled HDPE. The polyester-fibre mesh can also serve as nucleation sites, but the presence of the fibres and of the PE-g-MA compatibilizer slows the polymer-chain mobility during cooling, thus limiting the growth of crystals. The result was a composite with a lower crystallinity overall, but a relatively high melting temperature as compared to virgin HDPE .Interestingly, the melting temperature of the composite (142.3 °C) was slightly higher than that of r-HDPE. Although the overall crystalline content was decreased, this behavior indicates the presence of relatively stable crystalline domains in the matrix **(Faiz et al., 2014)**.Hence, the DSC results indicate that recycled HDPE was the dominant factor governing the crystallization kinetics and overall crystallinity, whereas the mesh-reinforced structure mainly influenced crystal organization and thermal stability. while the mesh-reinforced structure had a significant effect on the crystal organization and thermal stability **(Zhang et al., 2023).**

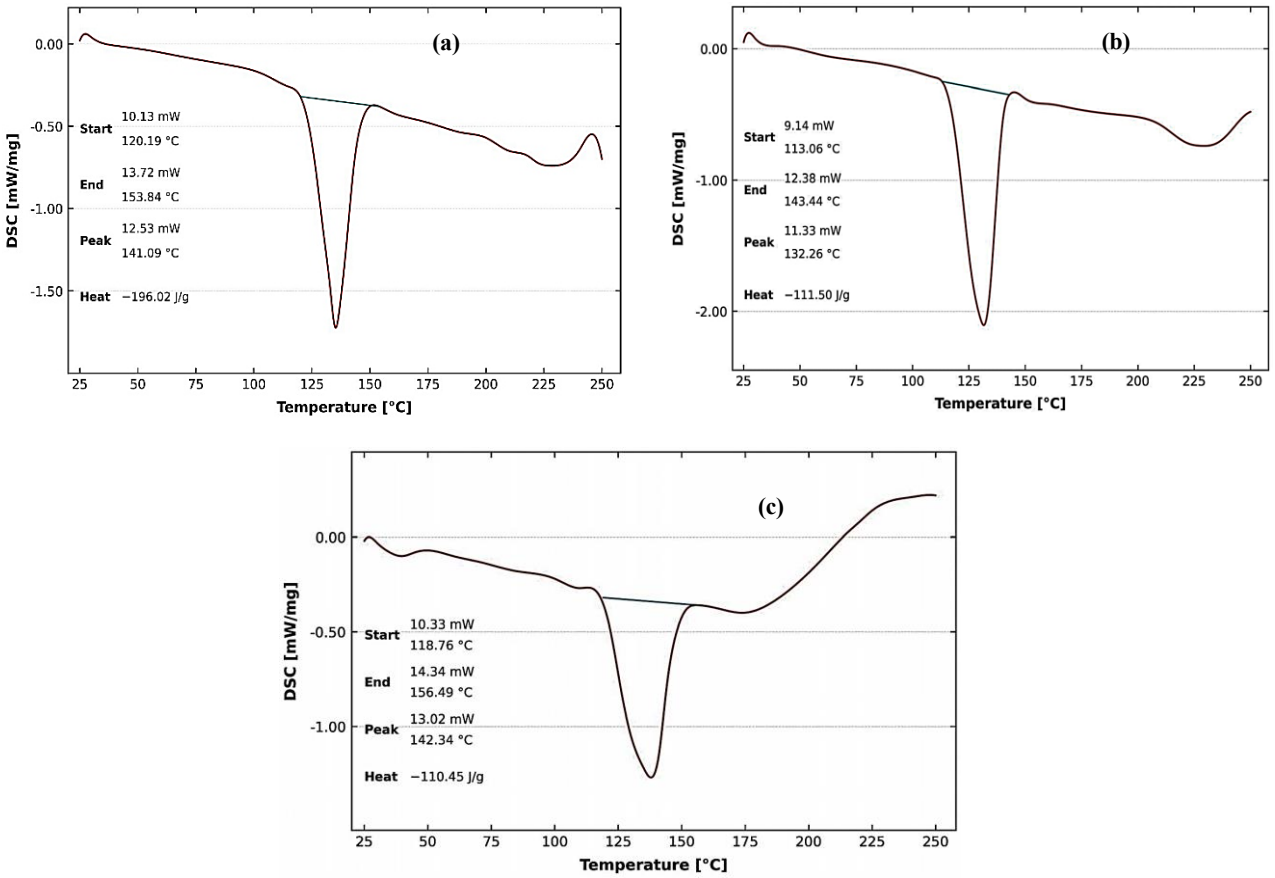

Figure 12. DSC thermograms of (a) virgin HDPE, (b) recycled HDPE, and (c) polyester fiber-reinforced composite.

4. CONCLUSIONS

In this study, the successful preparation of composites based on recycled polyester fibers and HDPE were shown, emphasizing the importance of reinforcement architecture in governing the mechanical properties of the composites. Among all investigated configurations, the mesh-reinforced composite exhibited the highest tensile strength and impact resistance (52 MPa and 487.8 J/m, respectively). This enhanced performance is associated with its intricate network of interconnected fibers, which enables more effective stress distribution and better resistance to crack propagation than standard fiber configurations. When recycled HDPE (r-HDPE) was used, there was a gradual decrease in performance, which is typical of what has been reported for recycled HDPE. This was supported by DSC analysis (as a reduction in crystallinity) and SEM (as an increase in matrix heterogeneity and micro-voids). The results indicate that r-HDPE affects the structural organization in the matrix, but the use of a mesh framework can help to overcome some of these drawbacks up to 20 wt.% of recycled content. Finally, the use of a structured mesh reinforcement and controlled recycled content is a promising pathway to recycling plastic and textile waste to sustainable engineering materials. Future studies should target long-term durability, environmental aging and direct characterization of interfacial interactions to further assess the industrial viability of the above composites. Despite the significant improvement achieved through mesh reinforcement and PE-g-MA compatibilization, the mechanisms governing interfacial adhesion and

recycled HDPE degradation were evaluated indirectly through mechanical, thermal, and morphological analyses. Additional rheological and molecular-level characterization would provide a deeper understanding of the structure–property relationships in these composites.

Credit Authorship Contribution Statement

Huda A Abdulimam: Conceptualization, Methodology, Investigation, Experimental work, Data curation, Formal analysis, Validation, Visualization, and Writing–original draft preparation.Hayder A. Abbood: Supervision, Data interpretation, Formal analysis support, Writing – review and editing, Scientific proofreading, and Final manuscript review.

Declaration of Competing Interest

The authors declare that they have no known competing financial interests or personal relationships that could have appeared to influence the work reported in this paper.

REFERENCES

Ajayi, N.E., Rusnakova, S., Ajayi, A.E., Ogunleye, R.O., Agu, S.O., and Amenaghawon, A.N., 2025. A comprehensive review of natural fiber reinforced polymer composites as emerging materials for sustainable applications. *Applied Materials Today, 43*, 102666. https://doi.org/10.1016/j.apmt.2025.102666

Al-Obaidi, Z., 2023. The assessment of using fiber produced from plastic broom bristles on the impact property of normal-weight concrete slabs. *Al-Qadisiyah Journal for Engineering Sciences*, 16(4), pp. 268–272. https://doi.org/10.30772/qjes.2023.163867.1690

Asim, M., Jawaid, M., Nasir, M., Saba, N., Shahroze, R. M., Sultan, M. T. H., Hamdan, S., Sandu, A. V., Khalina, A., and Jawaid, M., 2018. Thermal, physical properties and flammability of silane-treated kenaf/pineapple leaf fibres phenolic hybrid composites. *Composite Structures*, 202, pp. 1330–1338. https://doi.org/10.1016/j.compstruct.2018.06.068

ASTM D1895-96., 2010. *Standard test methods for apparent density, bulk factor, and pourability of plastic materials.* ASTM International. West Conshohocken, PA: Author. https://doi.org/10.1520/D1895-96R10

ASTM D256-10., 2010. *Standard test methods for determining the Izod pendulum impact resistance of plastics*. ASTM International. https://doi.org/10.1520/D0256-10

ASTM D570., 2018. *Standard test method for water absorption of plastics*. ASTM International. https://doi.org/10.1520/D0570-18

ASTM D638-14., 2014. *Standard test method for tensile properties of plastics*. ASTM International. https://doi.org/10.1520/D0638-14

ASTM D790-10., 2010. *Standard test methods for flexural properties of unreinforced and reinforced plastics and electrical insulating materials*. ASTM International. https://doi.org/10.1520/D0790-10

Asyraf, M., Khan, T., Syamsir, A., and Supian, A., 2022. Synthetic and natural fiber-reinforced polymer matrix composites for advanced applications. *Materials*, 15(17), P. 6030. https://doi.org/10.3390/ma15176030

Awad, A. H., El Gamasy, R., Abd El Wahab, A., and Abdellatif, M. H., 2019. Mechanical and physical properties of PP and HDPE. *Engineering Science*, 4(2), P. 34. https://doi.org/10.11648/j.es.20190402.12

Benhamadouche, L., Moussaoui, N., and Benkhelif, A., 2025. Resistance to crack propagation of a composite with recycled jute fabric–polypropylene. *Composite Structures*, 356, P. 118884.

Butylina, S., Martikka, O., and Kärki, T., 2011. Properties of wood fibre–polypropylene composites: Effect of wood fibre source. *Applied Composite Materials*, 18(2), pp. 101–111. https://doi.org/10.1007/s10443-010-9134-2

Chen, J., Pan, Z., Yang, S., Cao, C., Zhou, W., Xie, Y., Yang, Y., and Qian, Q., 2024. Highly filled waste polyester fiber/low-density polyethylene composites with a better fiber length retention fabricated by a two-rotor continuous mixer. *Polymers*, 16(20), P. 2929. https://doi.org/10.3390/polym16202929

Chen, L.-B., Huang, Y.-H., Liu, L., Zhao, X., Liu, Z.-Y., Yang, W., and Yang, M.-B., 2020. Effects of processing conditions on the structure and properties of fiber-reinforced thermoplastic composites during extrusion and molding. *Composites Part B: Engineering*, 197, 107770. https://doi.org/10.1016/j.compositesb.2020.107770

Choi, N.-W., Mori, I., and Ohama, Y., 2006. Development of rice husk–plastic composites for building materials. *Waste Management*, 26(2), pp. 189–194. https://doi.org/10.1016/j.wasman.2005.05.008

Douiri, L., Jdidi, H., Kordoghli, S., El Hajj Sleiman, G., and Béreaux, Y., 2024. Degradation indicators in multiple recycling processing loops of impact polypropylene and high-density polyethylene. *Polymer Degradation and Stability*, 219, 110617.

Edah, G. O., Atiba, J. O., and Fayomi, O. S. I., 2025. Advancements in fibre-reinforced polymers: Properties, applications (A mini review). *Next Materials*, 8, 100743. https://doi.org/10.1016/j.nxmate.2025.100743

Faiz, S., Anis, A., Luqman, M., and Al Zahrani, S. M., 2014. Studies on thermal, mechanical, morphological, and viscoelastic properties of polybenzimidazole fiber reinforced high-density polyethylene composites. *Polymer Composites*. https://doi.org/10.1002/pc.23148

Fox, C., Magrini, T., and Studart, A. R., 2025. Tailoring the fracture response of two-phase network reinforced composites. *International Journal of Solids and Structures*, 323, 113658.

Grande, C. and Torres, F.G. 2005. Investigation of fiber organization and damage during single screw extrusion of natural fiber reinforced thermoplastics. *Advances in Polymer Technology*, 24(4), pp. 289–299.

Gupta, M., and Singh, R., 2019. PLA-coated sisal fibre-reinforced polyester composite: Water absorption, static and dynamic mechanical properties. *Journal of Composite Materials*, 53(1), pp. 65–72. https://doi.org/10.1177/0021998318780227

Housmans, J. W., Gahleitner, M., Peters, G. W. M., and Meijer, H. E. H., 2009. Structure–property relations in molded, nucleated isotactic polypropylene. *Polymer*, 50(10), pp. 2304–2319. https://doi.org/10.1016/j.polymer.2009.02.050

Jawaid, M., Abdul Khalil, H. P. S., Noorunnisa Khanam, P., and Abu Bakar, A., 2011. Hybrid composites made from oil palm empty fruit bunches/jute fibres: Water absorption, thickness swelling and density behaviours. *Journal of Polymers and the Environment*, 19(1), pp. 106–109. https://doi.org/10.1007/s10924-010-0203-2

Jawaid, M., Thariq, M., and Saba, N., 2019. Mechanical and physical testing of biocomposites, fibre-reinforced composites, and hybrid composites. *Woodhead Publishing*. https://doi.org/10.1016/C2016-0-04437-6

Joseph, K., Thomas, S., and Pavithran, C., 1996. Effect of chemical treatment on the tensile properties of short sisal fibre-reinforced polyethylene composites. *Polymer*, 37(23), pp. 5139–5149. https://doi.org/10.1016/0032-3861(96)00144-9

Kaneyasu, H., Phanthong, P., Okubo, H., and Yao, S., 2021. Investigation of degradation mechanism from shear deformation and the relationship with mechanical properties, lamellar size, and morphology of high-density polyethylene. *Applied Sciences*, 11(18), P. 8436. https://doi.org/10.3390/app11188436

Kantz, M.R., Newman, H.D., and Stigale, F.H., 1972. The skin-core morphology and structure–property relationships in injection-molded polypropylene**.** *Journal of Applied Polymer Science***,** 16(5), pp. 1249–1260.

Kazayawoko, M., Balatinecz, J.J., and Matuana, L.M., 2009. The effects of polyethylene grafted maleic anhydride on the properties of wood fiber–recycled polyethylene composites. *Journal of Composite Materials*, 43(8), pp. 839–851. https://doi.org/10.1177/0021998309103089

Lima, P.S., Brito, R.S.F., Santos, B.F.F., and Wellen, R.M.R., 2017. Rheological properties of HDPE/chitosan composites modified with PE-g-MA. *Journal of Materials Research***,** 32(4), pp. 775–785.

Liu, Y., Xie, J., Wu, N., Wang, L., Ma, Y., and Tong, J., 2019. Influence of silane treatment on the mechanical, tribological, and morphological properties of corn stalk fiber reinforced polymer composites. *Tribology International*, 131, pp. 398–405. https://doi.org/10.1016/j.triboint.2018.11.004

Ma, Y., Ma, Q.-S., Suo, J., and Chen, Z.-H. 2008. Low-temperature fabrication and characterization of porous SiC ceramics using silicone resin as binder. *Ceramics International*, 34(2), pp. 253–255. https://doi.org/10.1016/j.ceramint.2006.08.018

Ngaowthong, C., Borůvka, M., Běhálek, L., Lenfeld, P., Švec, M., Dangtungee, R., Siengchin, S., Rangappa, S. M., and Parameswaranpillai, J., 2019. Recycling of sisal fiber reinforced polypropylene and polylactic acid composites: Thermo-mechanical properties, morphology, and water absorption behavior. *Waste Management*, 97, pp. 71–81. https://doi.org/10.1016/j.wasman.2019.07.038

Prajapati, R. S., Jain, S., and Shit, S. C., 2017. Development of basalt fiber-reinforced thermoplastic composites and effect of PE-g-MA on composites. *Polymer Composites*, 38(11), pp. 2443–2451.

Ragaert, K., Delva, L., and Van Geem, K., 2017. Mechanical and chemical recycling of solid plastic waste. *Waste Management*, 69, pp. 24–58. https://doi.org/10.1016/j.wasman.2017.07.044

Regazzi, A., Teil, M., Dumont, P. J. J., Harthong, B., Imbault, D., Peyroux, R., and Putaux, J. L., 2019. Microstructural and mechanical properties of biocomposites made of native starch granules and wood fibers. *Composites Science and Technology*, 182, 107755. https://doi.org/10.1016/j.compscitech.2019.107755

Savas, L.A., Tayfun, U., and Dogan, M., 2016. The use of polyethylene copolymers as compatibilizers in carbon fiber reinforced high-density polyethylene composites. *Composites Part B: Engineering*, 108, pp. 108–115.

Singh Bahra, M., Gupta, V. K., and Aggarwal, L., 2017. Effect of fibre content on mechanical properties and water absorption behaviour of pineapple/HDPE composite. *Materials Today: Proceedings*, 4(2), pp. 3207–3214. https://doi.org/10.1016/j.matpr.2017.02.206

Venkat Ramanan, A., and Rajamurugan, G., 2024. Significance of wire mesh reinforcement on carbon and glass fiber composite: A review. *Physica Scripta*, 99(10), P. 102003.

Wilczyński, K., Buziak, K., Wilczyński, K.J., and Lewandowski, A., 2018. Computer modeling for single-screw extrusion of wood–plastic composites. *Polymers*, 10(3), P. 295.

Xiao, K. and Tzoganakis, C., 2010. An experimental study of single-screw extrusion of HDPE–wood composites. *Advances in Polymer Technology*, 29(4), pp. 273–284.

Yamsaengsung, W., and Sombatsompop, N., 2009. Effect of chemical blowing agent on cell structure and mechanical properties of EPDM foam, and peel strength and thermal conductivity of wood/NR composite–EPDM foam laminates. *Composites Part B: Engineering*, 40(7), pp. 594–600. https://doi.org/10.1016/j.compositesb.2009.04.003

Zeng, S. F., Zhang, H. R., Li, Z. K., Hu, C. Y., and Wang, Z. W., 2023. Effect of mechanical recycling on crystallization, mechanical, and rheological properties of recycled high-density polyethylene and reinforcement based on virgin high-density polyethylene. *Journal of Applied Polymer Science*, 141(11), P. e55097. https://doi.org/10.1002/app.55097

تصنيع مركبات قائمة على البولي إيثيلين عالي الكثافة وتحسين خصائصها الميكانيكية من خلال الدمج التآزري لألياف البوليستر المهدرة والبولي إيثيلين عالي الكثافة

هدى عبدالرضا عبدالامام*، حيدر عبد الحسن عبود

قسم هندسة المواد، كلية الهندسة، جامعة البصرة، البصرة، العراق

الخلاصة

لقد حظي البولي إيثيلين عالي الكثافة المقوى بألياف البوليمر باهتمام كبير خلال العقود الأخيرة؛ إلا أن تطبيقه الفعال يتطلب تفاعلًا قويًا بين السطوح البينية للألياف والمصفوفة لضمان نقل فعال للإجهاد. يمكن أن يؤدي سوء تحضير المصفوفة إلى تكتل الألياف وضعف الارتباط بين السطوح، مما يؤثر سلبًا على الأداء الميكانيكي للبولي إيثيلين عالي الكثافة المقوى. في هذه الدراسة، تم تصنيع البولي إيثيلين عالي الكثافة المقوى بألياف البوليستر (PF) والمُتوافق مع البولي إيثيلين المطعّم بانهيدريد الماليك (PE-g-MA) باستخدام عملية بثق أحادية اللولب. في البداية، تم إنتاج المركبات بطبقة ألياف واحدة بنسب وزن مختلفة (0–20٪) لتحديد المحتوى الأمثل للتعزيز. وبعد ذلك، تمت دراسة اتجاهات مختلفة للألياف، بما في ذلك التكوينات بزوايا 0° و30° و45° و60° و90°، بالإضافة إلى التكوينات الشبكية والقصيرة والعشوائية. علاوة على ذلك، تم تقييم تأثير إدخال البولي إيثيلين عالي الكثافة المعاد تدويره (r-HDPE) بنسب وزن متماثلة. تم توصيف الخصائص الميكانيكية (الشد والانحناء والصدمات) والمورفولوجية (SEM) والحرارية (DSC) والفيزيائية بشكل منهجي. أظهر تكوين الألياف الشبكية أفضل أداء، حيث زادت قوة الشد بنسبة 126٪ (52 ميجا باسكال) وقوة الصدم بنسبة 138٪ (487.8 جول/م) مقارنةً بـ HDPE غير المقوى. ويُعزى هذا التحسن إلى تحسين نقل الحمل وآليات فعالة لمنع التشقق، مدعومة بكثافة أعلى ومسامية أقل. ومع ذلك، أدى زيادة محتوى r-HDPE إلى انخفاض تدريجي في الأداء الميكانيكي، خاصةً فوق نسبة 20٪. وتُظهر هذه النتائج جدوى إنتاج مواد بلاستيكية معززة عالية الأداء ومصنوعة من النفايات، مع فوائد بيئية وصناعية واعدة.

الكلمات المفتاحية: بولي اثلين عالي الكثافة، بولي اثلين عالي الكثافة معاد تدويرة، ألياف البوليستر المهدرة، بلاستيك معاد تدويرة